Article:
Fang, Hanlin, Liu, Jin, Lin, Qiaoling et al. (2019) Laser-Like Emission from a Sandwiched MoTe2 Heterostructure on a Silicon Single-Mode Resonator. Advanced Optical Materials. 1900538. ISSN: 2195-1071

https://doi.org/10.1002/adom.201900538

Laser-like emission from a sandwiched $MoTe_2$ heterostructure on a silicon single mode resonator

Hanlin Fang, Jin Liu, Qiaoling Lin, Rongbin Su, Yuming Wei, Thomas F. Krauss, Juntao Li, Yue Wang*, Xuehua Wang*

H. Fang, Prof. J. Liu, Q. Lin, Dr. R. Su, Y. Wei, Prof. J. Li, Prof. X. Wang
State Key Laboratory of Optoelectronic Materials and Technologies
School of Physics
Sun Yat-Sen University
Guangzhou, 510275, China
Email: lijt3@mail.sysu.edu.cn

Prof. T. F. Krauss, Dr. Y. Wang
Department of Physics
University of York
York, YO10 5DD, UK
Email: yue.wang@york.ac.uk

Keywords: single mode operation, $MoTe_2$, laser-like emission, hBN encapsulation, robustness

Abstract: Molybdenum ditelluride ($MoTe_2$) has recently shown promise as a gain material for silicon photonics. Reliable single mode operation and material stability remain two of the major issues that need to be addressed to advance this exciting technology, however. Here, we report laser-like emission from a sandwiched $MoTe_2$ heterostructure on a silicon single mode resonator. The heterostructure consists of a layer of $MoTe_2$ sandwiched between thin films of hexagonal boron nitride (hBN). It is known that tellurium compounds are sensitive to oxygen exposure, which leads to rapid degradation of the exposed layers in air. By encapsulating the $MoTe_2$ gain material, we observe much improved environmental stability. Using a recently introduced single mode resonator design, we are able to exercise better control over the mode spectrum of the cavity and demonstrate single mode operation with a wide free spectral range. At

room temperature, we achieve a Q-factor of 4500 and a threshold of 4.2 kW cm^{-2} at 1319 nm wavelength. These results lend further support to the paradigm of 2D material-based integrated light sources on the silicon platform.

1. Introduction

Silicon is now firmly established as a photonic material, yet a simple, low-cost technology for integrating gain material and for fabricating light emitters is still missing. The currently leading approach is to bond III-V materials onto the silicon, [1-3] however this method is difficult and expensive. As an alternative, there has been growing interest in the integration of 2D materials with silicon.[4] This approach can potentially be integrated into the CMOS workflow at very low cost, as many 2D materials can now be grown using wafer-scale fabrication techniques such as chemical vapor deposition (CVD).[5] The transition metal dichalcogenides (TMDs), as a member of the 2D materials family, show a number of interesting properties to meet the needs for making a silicon light emitter. Firstly, compared to traditional semiconductors, TMDs have a high exciton binding energy in the order of 500 meV. [6, 7] This allows excitons to be readily observed even at room temperature, and also leads to a short spontaneous emission lifetime in the picosecond range.[8] Secondly, compared to traditional quantum wells, various TMDs can be stacked to construct 2D heterostructures without the need for lattice matching.[9] This has already been exploited for the fabrication of 2D TMDs based electrically-driven LEDs and detectors.[10-12] Finally, some of the 2D material family have been shown to emit in the silicon transparency window, especially in the technologically important communication band around 1300 nm.[13] Here, we exploit

all of these properties by creating a heterostructure stack consisting of hBN-$MoTe_2$-hBN. $MoTe_2$ is the only TMD demonstrated so far that supports resonant emission in the 1300 nm regime. By creating a sandwich structure, we can avoid some environmental stability issues, as it is known that bare $MoTe_2$ flakes exhibit degradation in a matter of days when exposed to air.[14]

The TMD stack is then placed onto a cavity to resonantly enhance the light emission and to achieve lasing. As an aside, it has recently been discussed [15, 16] that laser operation from a TMD on a resonator is yet to be convincingly demonstrated, mainly due to the existing devices failing to meet the quantum threshold and the coherence criteria.

In order to achieve lasing, the cavity requires both a high quality factor and good heat-sinking. This combination of requirements excludes the use of conventional photonic crystal designs as they are typically based on an airbridge geometry. Even the recently introduced bound states in the continuum designs also benefit from the refractive index symmetry provided by airbridges. Furthermore, the cavity should only support a single resonant mode with a large free spectral range; the large free spectral range requirement stems from the relatively large gain bandwidth of the TMDs. This requirement excludes the micro-disk/ring resonator geometry and also makes the conventional photonic crystal nanobeam geometry unsuitable, where the resonant mode may sit relatively close to a band-edge mode. As a result, we investigate further a recently introduced nanocavity design,[17] which gives more degrees of freedom for achieving single mode operation, especially via the suppression of band-edge states.

2. **Design and Fabrication**

A schematic diagram and an optical micrograph of our device are shown in **Figure 1**a. The $MoTe_2$ is exfoliated using the standard scotch tape method.[18-20] The heterostructure consisting of hBN/$MoTe_2$/hBN is then fabricated using the van der Waals pick-up method [21, 22] and is transferred onto the silicon cavity (Figure 1b, see methods for more details). It is now well known that $MoTe_2$ degrades when directly exposed to air, hence encapsulating it between layers of hBN enhances its environmental stability.[10, 23] By protecting the $MoTe_2$ layer with hBN, we have not observed any degradation of the device performance after exposure to air for a week, confirming the observations of Y. Bie et al.[10]. In contrast, un-encapsulated devices need to be stored in vacuum to maintain their performance. On the other hand, it is known that hBN encapsulation reduces the PL linewidth of monolayer $MoTe_2$.[24-26] We also observe slight spectral narrowing of the monolayer $MoTe_2$ emission following hBN encapsulation, yet we do not observe this phenomenon in the few-layer material. Further details about the influence of hBN encapsulation on $MoTe_2$ is shown in sections B and C of the supporting information.

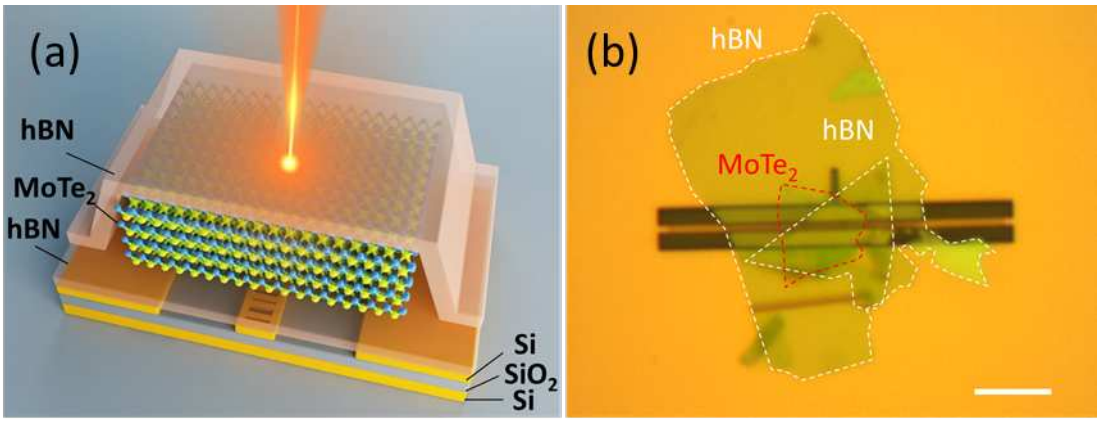

Figure 1. (a) Schematic diagram of the hBN-$MoTe_2$-hBN sandwich placed on the silicon single mode cavity. A few-layer thick flake of $MoTe_2$ provides the optical gain. The $MoTe_2$ flake is sandwiched between two layers of hBN and is placed on the cavity. (b) Optical microscope image of the fabricated structure. The $MoTe_2$ and hBN layers are marked by red and white dashed lines, respectively. The scale bar is 5 μm.

The design of the silicon single mode cavity is inspired by a previous report, [17] which was based on GaAs and operated around 1000 nm. We optimized the parameters for our silicon-on-silica geometry and for 1300 nm operation wavelength, to meet the needs for a light source in the technologically important 1300 nm data communications band. **Figure 2**a shows a schematic diagram of this structure, which uses two distinct 1D photonic crystal mirrors. These mirrors follow a design whereby d_i (i = 0, 1, 2) and a are the diameter and period of the holes, respectively. Using 3D FDTD simulation (Figure 2c), we determine a Q-factor of Q=15045 for the parameter set of d_0 = 0.25a, d_1 = 0.2a and d_2 = 0.3a, with which only one confined mode exists in the common bandgap (75 nm) of the two mirrors. This Q-factor is lower than that of a corresponding membrane structure (Q=35300), but the addition of the 2D material typically limits the cavity to a Q-factor of a few thousand anyway. [27-32] Therefore, the mechanical stability and the heat dissipation provided by the silica substrate are more important than achieving a super high “cold-cavity” Q-factor.

Figure 2 also highlights the key advantage of this design compared to the conventional photonic crystal nanobeam design. Both designs give a truly single mode cavity with a large intrinsic free spectral range. The free spectral range of the device is not limited by the cavity itself, however, by the mirrors. In the case of conventional photonic crystal design, the band-edge states of the mirrors limit the free spectral range. In contrast, these band-edge states are effectively suppressed by the new design, which therefore offers a much larger effective free spectral range (Figure 2d).

3. Experiments

The cavity was fabricated by electron beam lithography on a 220 nm silicon-on-insulator (SOI) wafer, based on the design in Figure 2a. After transferring the 2D material heterostructure onto the cavity (Figure 2b), we measured the photoluminescence (PL) spectrum using a 785 nm pump laser. Only a single mode peak at the wavelength of 1319 nm was observed, confirming the large free spectral range of the cavity, together with the background PL peaking at 1170 nm. We note that the PL of the trion appears to be the main contributor to the optical gain, mainly because the trion line is broader than the exciton line [33] (see section D of supporting information for details). However, the energies of the exciton and the trion are relatively far from the observed cavity-based emission wavelength of 1319 nm, which suggests that there may be additional extrinsic contributors to the emission process, such as defects and phonon modes. The thickness of $MoTe_2$ is measured to be 4 layers by optical contrast and AFM. Please see section A of the supporting information for further information on the determination of the thickness of the $MoTe_2$ flakes.

We note that this result builds on previous work[32] that has demonstrated multimode lasing from $MoTe_2$ on a traditional nanobeam cavity. In comparison, the novelty of our work can be summarized as follows: Firstly, we demonstrate single mode operation from a TMD-on-cavity system over a much wider free spectra range. Secondly, our cavity is supported by a silica layer, instead of being suspended in air, which significantly improves structural robustness and heatsinking.

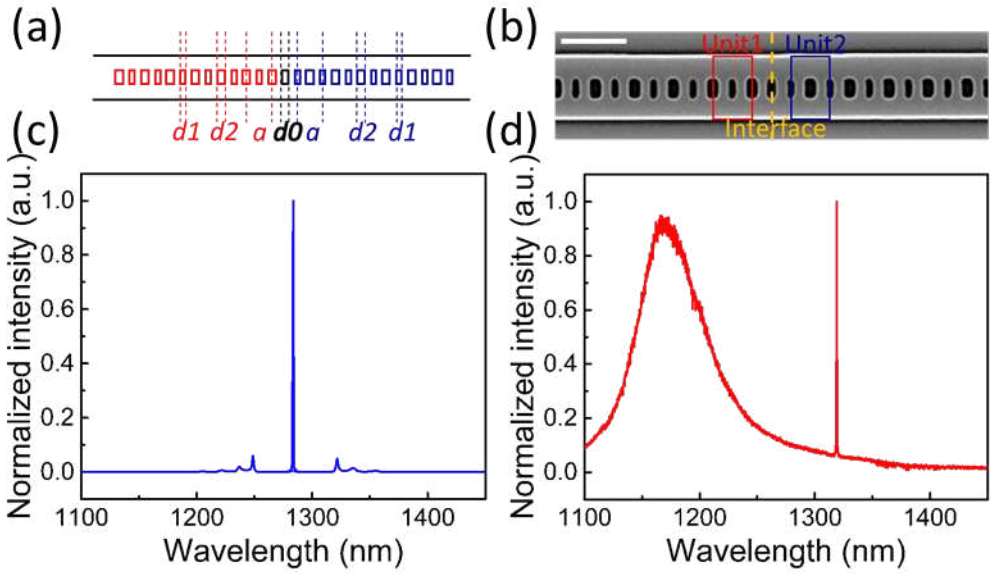

Figure 2. Silicon single mode cavity. (a) The design of the square hole-based cavity. (b) Scanning electron microscope (SEM) image of a fabricated 1D nanocavity. The scale bar is 500 nm. (c) Calculated transmission spectrum of the cavity. (d) Micro-PL measurement performed at room temperature, highlighting the single mode nature of the resonant cavity. Please note that the cavity was not far-field optimized, hence the out-of plane emission from the cavity mode is very weak and appears orders of magnitude weaker in the observed spectrum than it actually is.

We then studied the emission properties further using a micro-PL setup with a cw pump laser at 785 nm wavelength. **Figure 3**a shows the light in – light out curve (also known as the L-L curve). We observe a nonlinear dependence on the pump power that is distinctly different from the linear dependence seen away from the cavity (not shown), with an obvious kink at the threshold P_{th} of ~4.2 kW cm^{-2}. This value is very similar to

other 2D material based laser-like emitters.[28] Figure 3b shows the PL spectra with pump powers below and above this threshold.

To further demonstrate the properties of the laser-like emission, we plot the integrated intensity and the linewidth of the cavity mode as a function of pump power density in Figure 3c and 3d. The L-L curve in log-log regime shows the characteristics S-shape (see Figure 3c), which is a typical feature for lasing. In Figure 3d, linewidth narrowing can be observed when increasing the pump power density and we determine a maximum Q-factor of 4486 using a Lorentzian fit of the cavity mode when above threshold, corresponding to a FWHM of 0.294 nm with a pump power density of 10.29 kW cm^{-2}. The blue shaded areas in Figure 3c and 3d present the phase transition when the lasing action happens. This smooth transition originates from a high spontaneous emission coupling factor β of 0.2, which is obtained by fitting the experimental data to the laser rate equations (see section E of supporting information for more details).

We also note that thermal rollover starts occurring at approx. $3.5P_{th}$, which is significantly higher than that of emitters on membraned photonic crystal cavities previously studied. [28] This higher rollover value highlights the better heatsinking properties provided by the bottom silica cladding layer used here.

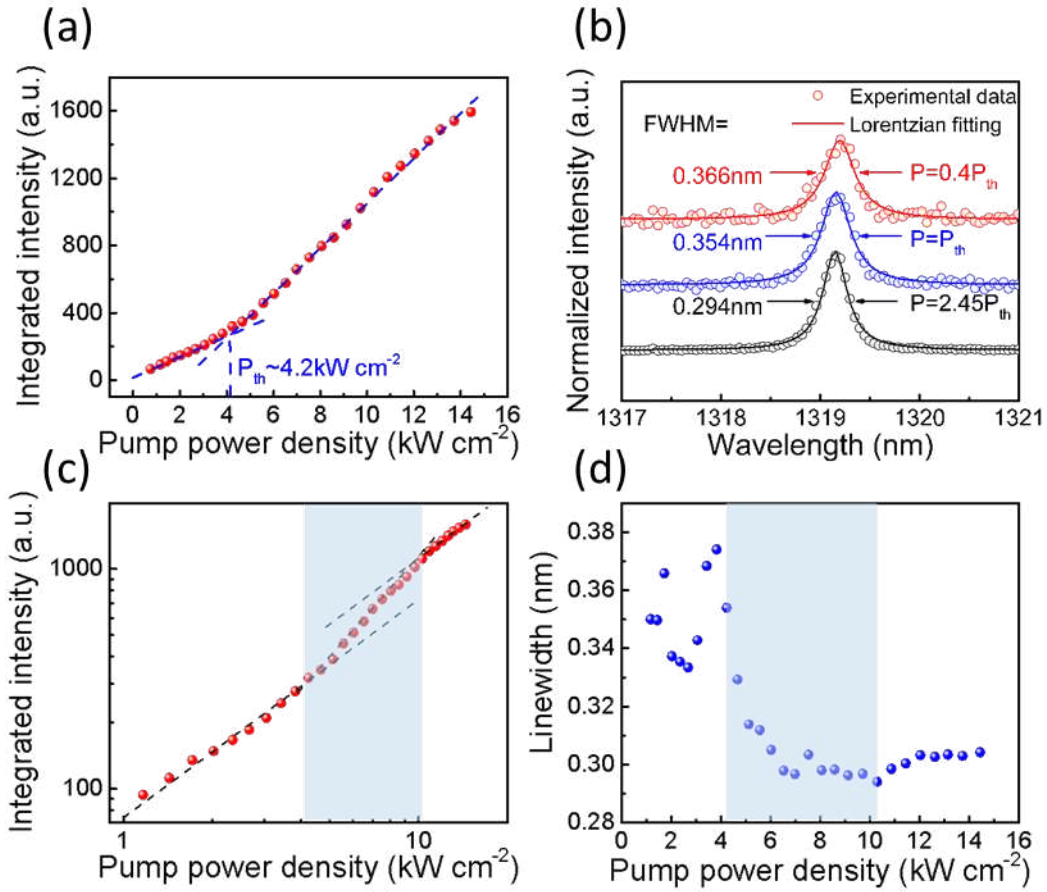

Figure 3. (a) L-L curve showing the output intensity of the resonant mode versus pump power. The crossover point of the blue dashed lines indicates a threshold of ~4.2 kW cm^{-2}. (b) PL spectra obtained for different pump power excitations. The lines and circles represent a Lorentzian fit and the experimental data, respectively. (c) Log-log plot of the output intensity as a function of pump power density. (d) Linewidth and peak intensity of the output mode as a function of pump power density.

4. Discussion and conclusions

In summary, we have demonstrated room temperature laser-like emission from few-layer $MoTe_2$ gain material that has been sandwiched between layers of hBN. The hBN provides protection from atmospheric oxygen and allows us to observe lasing action over extended periods of time without further encapsulation. The $MoTe_2$ is placed on the single mode cavity to provide the necessary feedback. The cavity features a very large free spectral range of over 300 nm, which is not achievable with a conventional photonic crystal nanobeam because of the band-edge states. The band-edge states are

effectively suppressed by the design used here. Furthermore, this design includes the bottom silica cladding, which provides much better heatsinking than air-bridge approaches, as evidenced by a much higher thermal roll-over than previously observed. Overall, we achieve single mode laser-like emission at 1310 nm, i.e. 140 nm away from the photoluminescence peak at 1170 nm, with no other modes present in the spectrum. While trions appear to be the major contributor to the observed gain, there may be other extrinsic factors, such as defects and phonon modes. Regarding laser action, we note that better evidence could be provided by determining the second order correlation function, but these can not be currently performed because of the limited time-resolution of our detector [15]. Overall, this 2D material heterostructure single mode laser design offers the blueprint for a potential silicon-integrated light emitter, which provides a very exciting prospect for future use in telecommunications, chemo- and bio-sensing and other applications.

5. Materials and Methods

Device fabrication. The cavities were fabricated using standard electron beam lithography and dry etching techniques. The pattern is first defined in ZEP520A resist by e-beam lithography, and then transferred to the silicon membrane by inductively coupled plasma etching. The resist residues are removed in hot N-Methyl-2-pyrrolidone (NMP).

The 2D heterostructures on SiO_2/Si substrate are made as follows. Firstly, the bottom hBN layer, the active $MoTe_2$ flake and the top hBN layer are exfoliated individually

onto separate SiO_2/Si substrates. Secondly, the 2D heterostructure is obtained by attaching a polypropylene carbonate (PPC) film onto PDMS and picking up the top hBN, $MoTe_2$ and bottom hBN layers in sequence. The adhesion relation from strong to weak is: PPC-hBN > hBN-SiO_2 > hBN-$MoTe_2$ > $MoTe_2$-SiO_2. Finally, we transfer this 2D heterostructure onto the cavity.

*Optical measurement***.** To optically excite the gain material, a 785 nm cw laser was focused through a 100x objective (NA = 0.85) onto the active gain material. The spectra were collected through the same objective onto an IR spectrometer with a 600 line/mm grating (Princeton Instrument SP2758), which has a spectral resolution of 0.2 nm and is coupled to a nitrogen-cooled CCD (Princeton Instrument OMA-V:1024/LN).

Supporting Information

Supporting Information is available from the Wiley Online Library or from the author.

Conflict of interest

The authors declare no conflict of interest.

Acknowledgements

This work is supported by National Key R&D Program of China (2016YFA0301300), National Natural Science Foundation of China (11761131001, 91750207, 11674402, 11761141015), Guangzhou Science and Technology projects (201805010004),

Natural Science Foundation of Guangdong (2016A030312012), National Supercomputer Center In Guangzhou, the Fundamental Research Funds for the Central Universities, and the EPSRC of the UK, Grant EP/M015165/1 (Ultrafast Laser Plasma Implantation- Seamless Integration of Functional Materials for Advanced Photonics).

References

[1] Z. Wang, A. Abbasi, U. Dave, A. De Groote, S. Kumari, B. Kunert, C. Merckling, M. Pantouvaki, Y. Shi, B. Tian, K. Van Gasse, J. Verbist, R. Wang, W. Xie, J. Zhang, Y. Zhu, J. Bauwelinck, X. Yin, Z. Hens, J. Van Campenhout, B. Kuyken, R. Baets, G. Morthier, D. Van Thourhout, G. Roelkens, *Laser Photon. Rev.* **2017**, *11*, 1700063.

[2] D. Liang, J. E. Bowers, *Nat. Photon.* **2010**, *4*, 511.

[3] Z. Zhou, B. Yin, J. Michel, *Light Sci. Appl.* **2015**, *4*, e358.

[4] N. Youngblood, M. Li, *Nanophotonics* **2017**, *6*.

[5] L. Zhou, K. Xu, A. Zubair, A. D. Liao, W. Fang, F. Ouyang, Y. H. Lee, K. Ueno, R. Saito, T. Palacios, J. Kong, M. S. Dresselhaus, *J. Am. Chem. Soc.* **2015**, *137*, 11892.

[6] T. C. Berkelbach, M. S. Hybertsen, D. R. Reichman, *Phys. Rev. B* **2013**, *88*.

[7] A. Chernikov, T. C. Berkelbach, H. M. Hill, A. Rigosi, Y. Li, O. B. Aslan, D. R. Reichman, M. S. Hybertsen, T. F. Heinz, *Phys. Rev. Lett.* **2014**, *113*, 076802.

[8] M. Palummo, M. Bernardi, J. C. Grossman, *Nano Lett.* **2015**, *15*, 2794.

[9] G. Fiori, F. Bonaccorso, G. Iannaccone, T. Palacios, D. Neumaier, A. Seabaugh, S. K. Banerjee, L. Colombo, *Nat. Nanotechnol.* **2014**, *9*, 768.

[10] Y. Q. Bie, G. Grosso, M. Heuck, M. M. Furchi, Y. Cao, J. Zheng, D. Bunandar, E. Navarro-Moratalla, L. Zhou, D. K. Efetov, T. Taniguchi, K. Watanabe, J. Kong, D. Englund, P. Jarillo-Herrero, *Nat. Nanotechnol.* **2017**, *12*, 1124.

[11] Y. Zhu, Z. Li, L. Zhang, B. Wang, Z. Luo, J. Long, J. Yang, L. Fu, Y. Lu, *ACS Appl. Mater. Interfaces* **2018**, *10*, 43291.

[12] J. Shang, C. Cong, L. Wu, W. Huang, T. Yu, *Small Methods* **2018**, *2*, 1800019.

[13] Y. Ota, R. Moriya, N. Yabuki, M. Arai, M. Kakuda, S. Iwamoto, T. Machida, Y. Arakawa, *Appl. Phys. Lett.* **2017**, *110*, 223105.

[14] B. Chen, H. Sahin, A. Suslu, L. Ding, M. I. Bertoni, F. M. Peeters, S. Tongay, *ACS Nano* **2015**, *9*, 5326.

[15] L. Reeves, Y. Wang, T. F. Krauss, *Advanced Optical Materials* **2018**, *6*, 1800272.

[16] C. Javerzac-Galy, A. Kumar, R. D. Schilling, N. Piro, S. Khorasani, M. Barbone, I. Goykhman, J. B. Khurgin, A. C. Ferrari, T. J. Kippenberg, *Nano Lett.* **2018**, *18*, 3138.

[17] Y. Ota, R. Katsumi, K. Watanabe, S. Iwamoto, Y. Arakawa, *Commun. Phys.* **2018**, *1*. 86.

[18] J. Bohr, *EPL* **2015**, *109*, 58004.

[19] D. M. Tang, D. G. Kvashnin, S. Najmaei, Y. Bando, K. Kimoto, P. Koskinen, P. M. Ajayan, B. I. Yakobson, P. B. Sorokin, J. Lou, D. Golberg, *Nat. Commun.* **2014**, 5, 3631.

[20] M. Yi, Z. Shen, *J. Mater. Chem. A* **2015**, *3*, 11700.

[21] L. Wang, I. Meric, P. Y. Huang, Q. Gao, Y. Gao, H. Tran, T. Taniguchi, K.

Watanabe, L. M. Campos, D. A. Muller, J. Guo, P. Kim, J. Hone, K. L. Shepard, C. R. Dean, *Science* **2013**, *342*, 614.

[22] P. J. Zomer, M. H. D. Guimarães, J. C. Brant, N. Tombros, B. J. van Wees, *Appl. Phys. Lett.* **2014**, *105*, 013101.

[23] G. H. Lee, X. Cui, Y. D. Kim, G. Arefe, X. Zhang, C. H. Lee, F. Ye, K. Watanabe, T. Taniguchi, P. Kim, J. Hone, *ACS Nano* **2015**, *9*, 7019.

[24] F. Cadiz, E. Courtade, C. Robert, G. Wang, Y. Shen, H. Cai, T. Taniguchi, K. Watanabe, H. Carrere, D. Lagarde, M. Manca, T. Amand, P. Renucci, S. Tongay, X. Marie, B. Urbaszek, *Phys. Rev. X* **2017**, *7*, 021026.

[25] B. Han, C. Robert, E. Courtade, M. Manca, S. Shree, T. Amand, P. Renucci, T. Taniguchi, K. Watanabe, X. Marie, L. E. Golub, M. M. Glazov, B. Urbaszek, *Phys. Rev. X* **2018**, *8*, 031073.

[26] J. Wierzbowski, J. Klein, F. Sigger, C. Straubinger, M. Kremser, T. Taniguchi, K. Watanabe, U. Wurstbauer, A. W. Holleitner, M. Kaniber, K. Muller, J. J. Finley, *Sci. Rep.* **2017**, *7*, 12383.

[27] S. Wu, S. Buckley, J. R. Schaibley, L. Feng, J. Yan, D. G. Mandrus, F. Hatami, W. Yao, J. Vuckovic, A. Majumdar, X. Xu, *Nature* **2015**, *520*, 69.

[28] Y. Ye, Z. J. Wong, X. Lu, X. Ni, H. Zhu, X. Chen, Y. Wang, X. Zhang, *Nat. Photon.* **2015**, *9*, 733.

[29] O. Salehzadeh, M. Djavid, N. H. Tran, I. Shih, Z. Mi, *Nano Lett.* **2015**, 15, 5302.

[30] J. Shang, C. Cong, Z. Wang, N. Peimyoo, L. Wu, C. Zou, Y. Chen, X. Y. Chin, J. Wang, C. Soci, W. Huang, T. Yu, *Nat. Commun.* **2017**, *8*, 543.

[31] H. Fang, J. Liu, H. Li, L. Zhou, L. Liu, J. Li, X. Wang, T. F. Krauss, Y. Wang, *Laser Photon. Rev.* **2018**, *12*, 1800015.

[32] Y. Li, J. Zhang, D. Huang, H. Sun, F. Fan, J. Feng, Z. Wang, C. Z. Ning, *Nat. Nanotechnol.* **2017**, *12*, 987.

[33] Z. Wang, H. Sun, Q. Zhang, J. Feng, J. Zhang, Y. Li, C. Ning, arXiv:1812.04296.

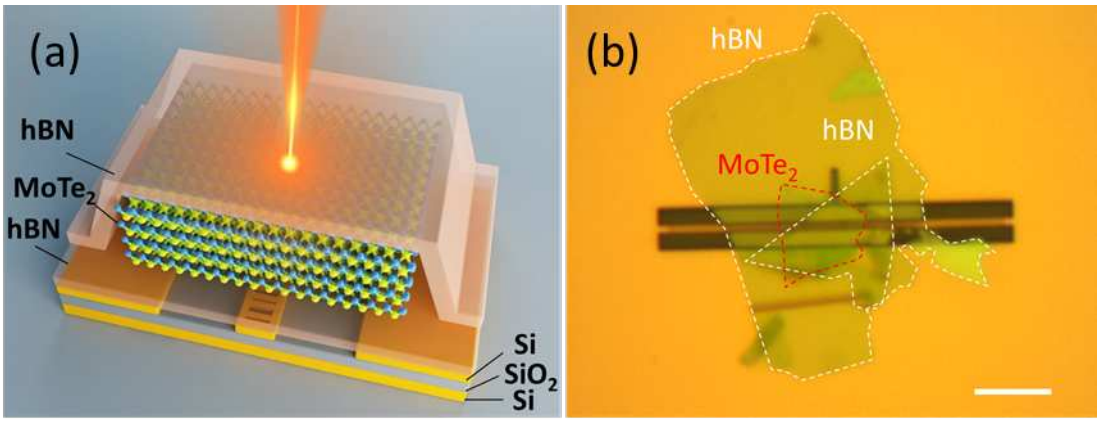

Figure 1. (a) Schematic diagram of the hBN-$MoTe_2$-hBN sandwich placed on the silicon single mode cavity. A few-layer thick flake of $MoTe_2$ provides the optical gain. The $MoTe_2$ flake is sandwiched between two layers of hBN and is placed on the cavity. (b) Optical microscope image of the fabricated structure. The $MoTe_2$ and hBN layers are marked by red and white dashed lines, respectively. The scale bar is 5 μm.

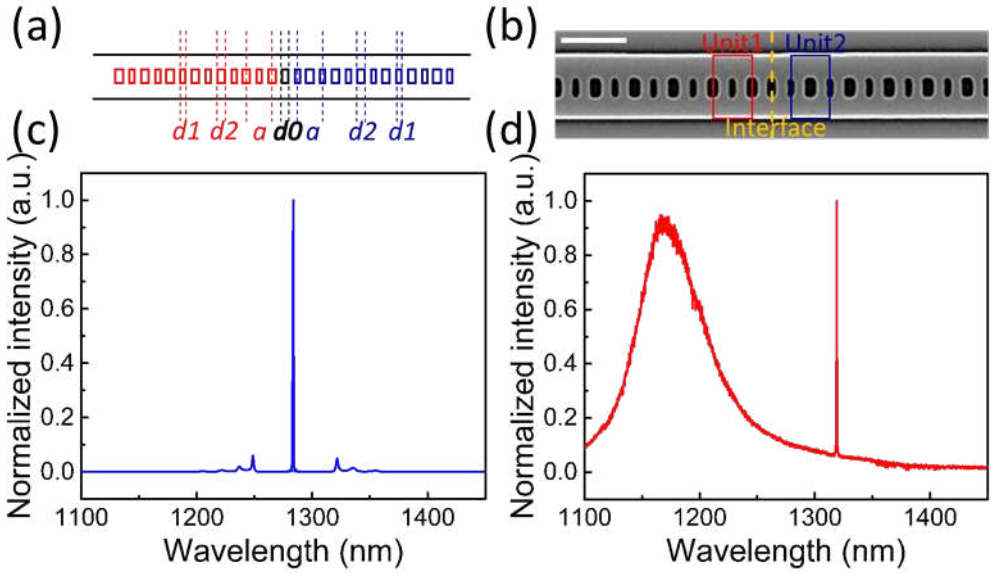

Figure 2. Silicon single mode cavity. (a) The design of the square hole-based cavity. (b) Scanning electron microscope (SEM) image of a fabricated 1D nanocavity. The scale bar is 500 nm. (c) Calculated transmission spectrum of the cavity. (d) Micro-PL measurement performed at room temperature, highlighting the single mode nature of the resonant cavity. Please note that the cavity was not far-field optimized, hence the out-of plane emission from the cavity mode is very weak and appears orders of magnitude weaker in the observed spectrum than it actually is.

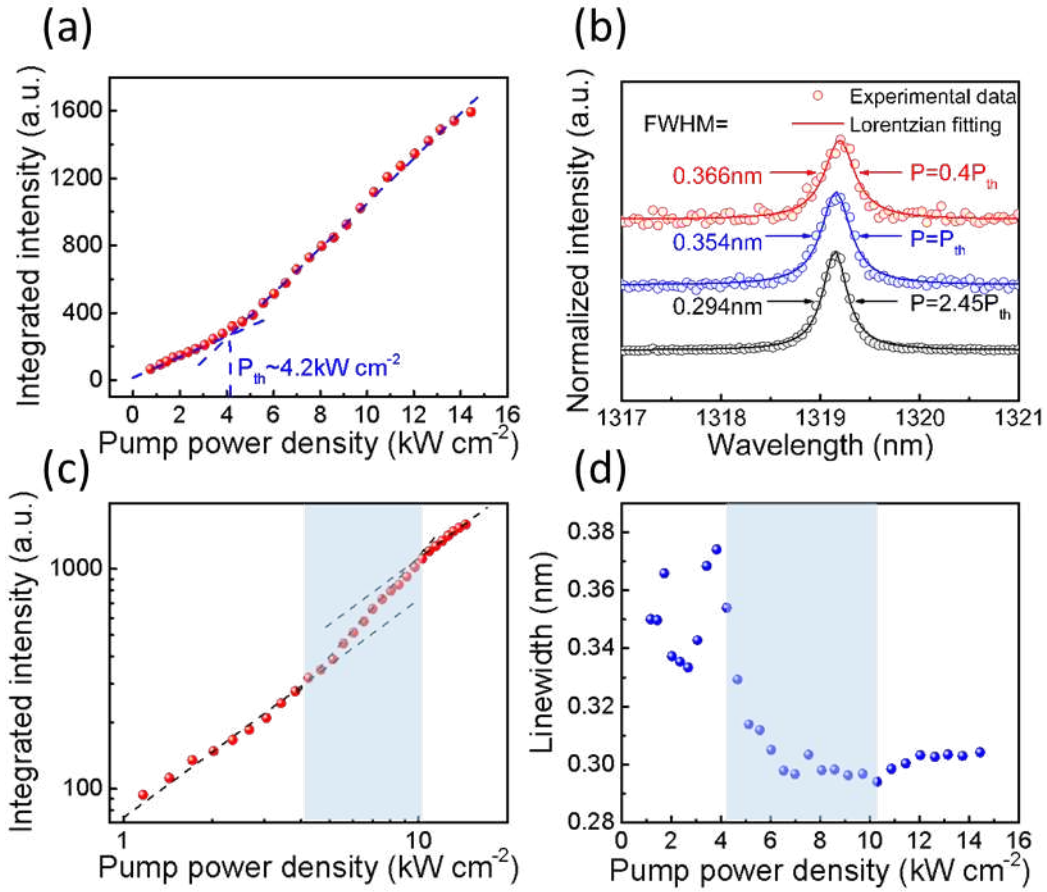

Figure 3. (a) L-L curve showing the output intensity of the resonant mode versus pump power. The crossover point of the blue dashed lines indicates a threshold of ~4.2 kW cm^{-2}. (b) PL spectra obtained for different pump power excitations. The lines and circles represent a Lorentzian fit and the experimental data, respectively. (c) Log-log plot of the output intensity as a function of pump power density. (d) Linewidth and peak intensity of the output mode as a function of pump power density.

Table of Contents

Text

This work demonstrates room temperature laser-like emission at 1319 nm, with single mode operation. The combination of hBN encapsulated $MoTe_2$ and un-menbraned photonic crystal nanobeam cavity give rise to a robust light emitting device. This design offers a feasible approach to realize an integrated light source on silicon platform.

Figure

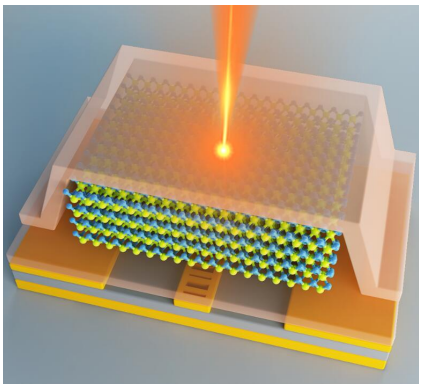

Keyword

single mode operation, $MoTe_2$, laser-like emission, hBN encapsulation, robustness